

Development of a drone-based evaluation tool for motion analysis in athletics long jump

Studienarbeit

im Studiengang

Informationstechnik

an der Dualen Hochschule Baden-Württemberg Mannheim

von

Name, Vorname: Faust, Jakob

Abgabedatum: 16.04.2024

Bearbeitungszeitraum: 17.10.2023 - 16.04.2024

Matrikelnummer, Kurs: 5507125, TINF21IT1

Betreuer: Jürgen Schultheis

Unterschrift Betreuer: _____

Mannheim, den

Contents

| | |
|---|------------|
| List of Figures | III |
| Listings | IV |
| List of acronyms | V |
| 1 Introduction | 1 |
| 2 Tasks | 3 |
| 3 Methodology | 5 |
| 3.1 Software fundamentals | 5 |
| 3.1.1 Programming Language and why Python | 5 |
| 3.1.2 Mediapipe for detecting body poses | 5 |
| 3.1.3 Why Mediapipe? | 7 |
| 3.1.4 OpenCV | 8 |
| 3.1.5 HDF5 file format | 8 |
| 3.2 GUI development | 9 |
| 3.2.1 Development framework Qt | 9 |
| 4 Implementation | 11 |
| 4.1 Long-jump analysis software | 11 |
| 4.1.1 Video processing | 12 |
| 4.1.2 Automatic takeoff frame detection | 18 |
| 4.1.3 Runtime considerations | 26 |
| 4.1.4 Visualization in a GUI | 26 |
| 4.2 Hardware setup | 26 |
| 4.2.1 Hardware selection | 27 |
| 4.2.2 Hardware assembly | 30 |
| Bibliography | VII |

List of Figures

| | | |
|------|---|----|
| 3.1 | Set of detectable body key points | 6 |
| 3.2 | HDF5 file structure | 9 |
| 4.1 | Long jump parameter overview | 12 |
| 4.2 | Video processing pipeline | 12 |
| 4.3 | Pose detection example | 15 |
| 4.4 | Knee angle calculation | 15 |
| 4.5 | Takeoff angle | 17 |
| 4.6 | Analyzed jumping parameters over time | 20 |
| 4.7 | Automatic takeoff frame detection results | 26 |
| 4.8 | Frame kit | 28 |
| 4.9 | Motor and ESC | 28 |
| 4.10 | General Wiring | 31 |
| 4.11 | UART wiring | 32 |
| 4.12 | UART data frame | 32 |

Listings

| | |
|---------------------------------|----|
| 4.1 Angle calculation | 16 |
|---------------------------------|----|

List of acronyms

AI Artificial Intelligence

BEC Battery Elimination Circuit

CM Center of mass

CPU Central Processing Unit

ESC Electronic Speed Control

FPV First Person View

GPS Global Positioning System

GPU Graphical Processing Unit

GUI Graphical User Interface

HAT Hardware Attached on Top

PDB Power Delivery board

PM Power Module

PWM Pulse Width Modulation

RPM Revolutions Per Minute

SSE Sum of Squared Errors

1 Introduction

Long jump is an athletic discipline that is renowned for its technical complexity and the precise movement patterns it demands from athletes. Even apparently small technical inaccuracies can significantly impact an athlete's performance. Moreover, as shown in [1] the forces during the take-off phase can reach up to 10 times the athlete's body weight, increasing the risk of serious injuries due to technical inaccuracies. Therefore, it is crucial to understand and continuously improve these movement patterns in training. However, taken the high approach velocity¹ into account, this can quickly become a difficult task. Especially the take-off phase can be very short and therefore hard to analyze.

Professional athletes often employ expensive high speed camera systems in combination with body pose markers to capture and analyze every single step they make.

Yet, this approach comes with some limitations. Due to their stationary installation, such camera systems are restricted to a fixed location. Moreover, they often combine multiple cameras like Murray et al. [2] used for sprint analysis in order to be able to capture the whole movement from the beginning of the approach until the landing. This leads to complex post-processing software requirements. Additionally, fixed markers need to be attached to an athletes body to be able to track their body position.

While these methods provide exact and reliable results, they are usually not accessible for hobby- and semi-professional athletes.

In recent years however the advances in Artificial Intelligence (AI) and especially within the area of deep neural network paved the way for analyzing methods that require less complex setups. As of 2023 deep neural networks trained for body pose detection are even used in medical applications like gait analysis [3]. Because of the already extremely high and continuously improving accuracy, its application within the area of motion analysis in long jump is treated in the scope of this work.

A semi-autonomous drone based evaluation tool is newly developed. It is supposed to offer a portable alternative to address the lack of existing opportunities in analyzing long jump performances in training. For this purpose, the drone should autonomously fly next

¹around 10 m/s in male semi-professional long jump

to the athlete throughout the whole jump, capturing their motion and therefore allow for a complete jump analysis. The drone itself is based on First Person View (FPV) drone hardware. It is build from scratch using an onboard single-board computer as flight control unit responsible for capturing the video. Additionally, a ground station software is developed to allow for a convenient jump analysis regarding the overall body pose as well as a fixed set of important parameters, i.e. knee angles, arm angles, hip position. The project's source code is available under <https://github.com/JF631/FLYJUMP>.

2 Tasks

This chapter provides an overview over all tasks that are approached in this project. Hardware related tasks are listed as well as software related tasks. Each main task is divided into several sub-tasks.

Task 1 Develop a platform independent computer software to analyze pre-recorded long-jump videos.

1. Integrate a body detection system.
2. Define an analysis output standard.
3. Develop an algorithm to automatically detect the take-off frame.
4. Implement a GUI to visualize analysis results.

Task 2 Build a quadcopter as hardware companion for recording long-jump videos. This specifically requires a camera as well as several sensors for navigation.

1. Select hardware components according defined criteria.
2. Build a flying quadcopter that is controllable from a ground station.
3. extend the quadcopter with a companion computer and a compatible camera to live stream videos.
4. test the camera accuracy.

Task 3 Implement a software that allows to control the drone from a ground station.

1. Set up a wireless connection to the quadcopter.
2. Define a communication protocol.
3. Integrate the control mechanism in the GUI.
4. Integrate a start measurement like mechanism.

Task 4 Develop a software to handle the incoming video livestream.

1. Establish a connection to the on-board companion computer.
2. Display the video frames in the GUI.

-
3. Offer the option for a rudimentary live analysis.

Task 5 Develop a software that can control the drone autonomously.

1. Establish between an on-board companion computer and PixHawk flight controller.
2. Implement an on-board body detection system.
3. Develop an auto-follow like controlling feature.

3 Methodology

The following chapter provides an overview over the relevant development components that are used within this project. Therefore, the used software packages are introduced before a short outline of the utilized drone hardware is given.

3.1 Software fundamentals

As the main part of this project's software will run on a portable remote computer allowing for not only to control the drone but also for performing the long jump analysis on video inputs, every software component is chosen to demand as little hardware requirements as possible. Especially no Graphical Processing Unit (GPU) is required to run the software. All image processing is performed using the Central Processing Unit (CPU) only. Furthermore, the software is designed to run platform independent.

3.1.1 Programming Language and why Python

Because of its interpreted nature and many cross-platform libraries, Python is one of the most used programming languages in the scientific area. Furthermore, it offers a high level of abstraction allowing for rapid prototyping approaches which is a key factor for this project. Besides fast implementation, Python nevertheless supports complex programming concepts like object-orientation.

Additionally, as stated in subsection 3.1.2 many machine learning and AI projects for detecting body poses have already been successfully implemented using Python.

Third party libraries and frameworks like *OpenCV* for image processing and *PyQt* for Graphical User Interface (GUI) development are widely used and therefore well documented. This leads to the decision to use Python as programming language within this work.

3.1.2 Mediapipe for detecting body poses

One of the software's main tasks is to perform a human body pose detection on video inputs. Because this part runs on the remote computer only, it can also handle pre-recorded

videos that should be evaluated.

The evaluation itself is performed using the Mediapipe framework. This framework uses a pre-trained convolutional neural network that is able to detect 33 key points in human body poses [4]. The network could theoretically even be fine-tuned to improve its accuracy on specific input types. Even if this so called *transfer-training* method requires significantly less training data compared to training a neural network from scratch, it is not applied within this project as first test runs already showed reliable results.

Furthermore, the Mediapipe framework does not require any hardware acceleration and is renowned for its precise output. Hii et al. for example showed in [3], [5] that the framework can be applied in medical gait analysis applications to replace marker based approaches. Moreover, Mediapipe offers three different detection models that differ in terms of speed and accuracy. The fastest detection model offers the lowest accuracy and vice versa.

Additionally, Mediapipe is optimized for multiple input types including videos and live streams, which is ideal for this project.

Figure 3.1 shows an overview of the 33 detectable key points.

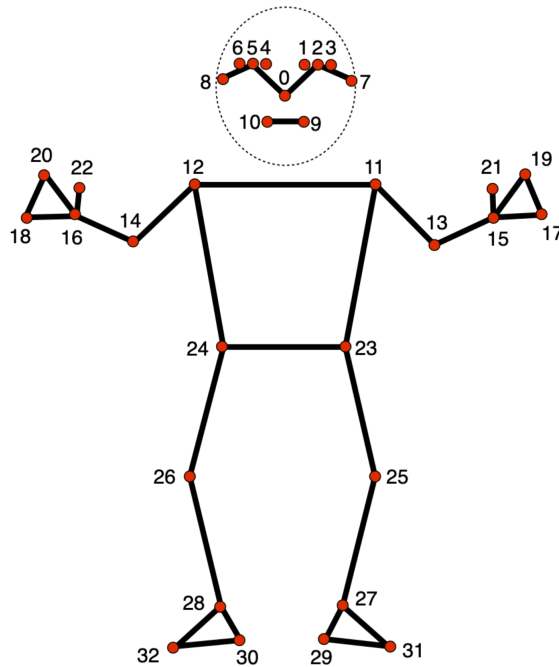


Figure 3.1: Fixed set of detectable body key points offered by the mediapipe framework [6]

Within this work, the key points in the head area (range [0 - 10]) are not of great interest apart from visualization purposes.

The knee, hip and arm key points however will be used for angle calculations and ground contact detection. Thus, a good performance in detecting the according key points within these areas is crucial for the software's overall reliability.

3.1.3 Why Mediapipe?

In recent years many approaches towards accurate body pose detection were developed and implemented. Many of those offer decent accuracies, but often lack reasonable performance, especially when no GPU is available for hardware acceleration. Following, two common alternatives to Mediapipe, namely OpenPose and AlphaPose, are shortly presented and differentiated from the chosen Mediapipe framework.

One of the most widely used human pose detection libraries is the open source library *OpenPose*. As shown in [7] it offers a Multi-Person pose estimation that is especially useful when dealing with groups of people. However, as this project is meant to be used for long jump evaluation, only one person needs to be tracked at a time. Even though OpenPose of course can handle one person pose estimation, mediapipe outperforms OpenPose in this area. Back in 2016 Kocabas et al. achieved around 23 FPS using GPU accelerated OpenPose pose detection [8] and Osokin later proposed an improved neural network design, allowing for up to 28 FPS without hardware acceleration [9]. As of 2023 these benchmarks are still reasonable. Mediapipe however achieves speeds of up to 63% higher.

While OpenPose uses a *Bottom-Up* approach due its multi-person application, Mediapipe uses the less computational complex *Top-Down* approach.

Bottom-Up implementations first detect all body key points present in an input image and then move on to grouping the recognized points in clusters. Points in the same cluster are then assigned to one person.

Top-Down approaches however first roughly detect the overall body position within the input image and then define a region of interest¹ around the subject. The following processing therefore only needs to take this defined region of interest into account, leading to significantly less computational complexity.

AlphaPose is another open source library often used for body pose estimation. Just like OpenPose it uses a Bottom-Up approach to reliable offer multi-person body pose detection. Additionally, AlphaPose, like Mediapipe, offers multiple detection models that differ regarding accuracy and speed. Again however, Mediapipe outperforms AlphaPose because of its Top-Down approach and because AlphaPose is designed to work with GPU acceleration, rather than running on CPU only.

Another advantage of Mediapipe is its output. While OpenPose and AlphaPose offer 2D coordinates for each detected key point, Mediapipe additionally offers a depth estimation resulting in a spatial 3D coordinate for each detected key point. Thereby, more comprehensive analysis can be performed.

¹sometimes also referred to as *Bounding Box*

3.1.4 OpenCV

OpenCV is an open source library commonly used for image processing in the area of computer vision and machine learning. It is written in C++, thus offering high performance in numerical operations, especially matrix operations.

`python-opencv` is the python wrapper for OpenCV which will be used in this project to efficiently read and process video frames. The python wrapper imports the underlying C++ functions as modules to take advantage of C++'s efficiency, resulting in significantly higher performance compared to equivalent Python only implementations. Furthermore, it is fully compatible with the `numpy` library, which allows for seamless conversion between `numpy` arrays and OpenCV image matrices.

3.1.5 HDF5 file format

To avoid analyzing the same jump, therefore the same video file, multiple times, the jump parameters should be saved after the analysis process alongside with the annotated video file, that visualizes the detected body pose (see Figure 3.1). Because parameters such as knee angles, arm angles, ground contact, etc. need to be stored frame-wise, a structured file format is suitable.

One common open source structured file format is HDF5. It is an acronym for Hierarchical Data Format (Version 5) and is very helpful to store large amounts of data as well as heterogeneous data. As the name already suggests, data is stored in a hierarchical, tree-like way.

A HDF5 tree mainly consists of three pre-defined components that allow to organize data in a file-system like fashion. The tree root, groups and datasets. *Groups* are folder-like structures that can either contain more groups or Datasets. *Datasets* hold the actual data that need to be stored.

Furthermore, each level (tree root, groups and datasets) can hold additional information via metadata. The metadata could for example contain information about metrics, timestamps or any other describing information. Therefore, each HDF5 file itself becomes a self-describing file that does not require any more than the included information to be interpreted correctly.

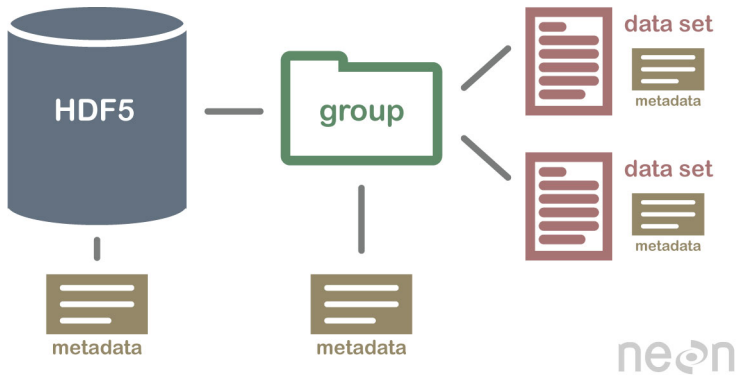


Figure 3.2: Principle HDF5 file structure ²

Within this work, one HDF5 file will be created per jump analysis. The frames are stored in a group each and the actual calculated parameters are saved group-wise as datasets.

3.2 GUI development

The software that is developed within this work should be useable on-field to allow for a fast analysis process. Besides the video analysis, the drone control should be embedded in the same software to always guarantee control over the drone.

Thus, a simple GUI is developed to offer a convenient drone control and video analysis process.

The GUI is developed using Qt and its Python binding PyQt. Both are presented in this section.

3.2.1 Development framework Qt

Qt is a development framework based on the programming language C++. It includes a GUI toolkit and therefore enables platform-independent application development. All common platforms including Linux, Windows and MacOS are supported by Qt. Additionally, both mobile operating systems, Android and iOS, are supported.

This project however will focus on the development of an application that is able to run under Windows, Linux and MacOS.

The Qt framework is mainly chosen because of its rich and comprehensive documentation³ and the availability of the well-supported Python binding *PyQt*.

As Qt is based on C++ all Qt source files are translated to C++ code. This step is

³<https://doc.qt.io/>

realized by the **Meta Object Compiler (MOC)** which is integrated as pre-processor. Thus, all Qt files are translated to so-called *Meta Object Code*, which can be seen as C++ source code with some enhancements. The most important enhancement is the signal and slot functionality which allows for an easy communication between different software and design elements (e.g. show a message dialog when a button is clicked).

Another important enhancement for this work is the convenient multi-threading management necessary for offering a responsive GUI even when cpu-bound calculations such as image processing is performed.

The GUI module PyQt

The discrepancy between Qt as C++ based framework and Python as chosen programming language for this project (as explained in subsection 3.1.1) can be overcome using Qt's Python binding PyQt. By using PyQt we can combine Python's machine learning advantages with Qt's platform-independent GUI development. More specifically *PyQt5*⁴ is used.

It allows building complex Qt applications using Python only instead of C++. All other described advantages that Qt offer remain valid despite the use of PyQt. Thus, the whole software within this project including the GUI can be developed using Python as programming language.

⁴<https://pypi.org/project/PyQt5/>

4 Implementation

This chapter focuses on the overall project's implementation. It mainly covers the four parts hardware assembly, long jump analysis, drone control and their consolidation into one GUI.

4.1 Long-jump analysis software

In order to analyze recorded long jump videos a ground station software is developed. Generally, the analysis is performed regarding the following set of parameters:

- left / right knee angle
- left / right arm angle
- takeoff angle
- left / right foot position
- hip height

These parameters are tracked over the whole jump, beginning with the run-up throughout the takeoff until the landing.

Figure 4.1 shows a detailed overview over the video data that can be analyzed by the software.

As the takeoff is (one of) the most important phases in a long jump, it is important to be able to detect the takeoff in a video. Such a takeoff detection is developed alongside the above-mentioned parameter detection- and calculation.

This section will first introduce the body key point detection process that is basis for all following calculations. Afterwards, an algorithm for an automatic takeoff frame detection based on a video input is implemented.

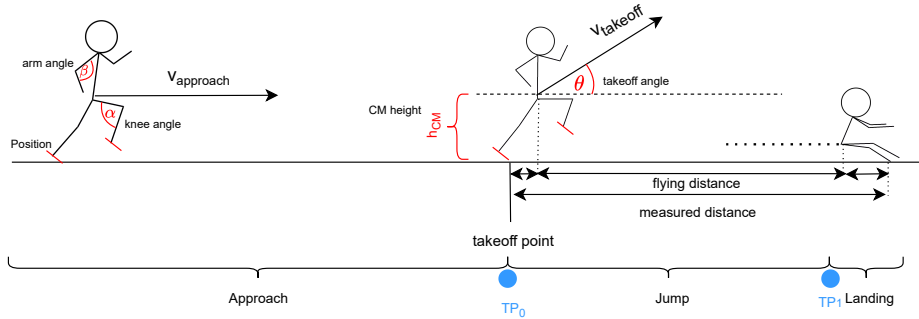


Figure 4.1: General long jump overview.

Parameters that can be analyzed are marked red.
 TP_0 and TP_1 denote phase transition points.

4.1.1 Video processing

After a video has been recorded, several processing steps need to be performed to calculate the parameters shown in Figure 4.1. All calculations are performed for each input video frame respectively. In the first processing stage, multiple filters can be applied to each frame. The body key point detection is then performed on the filtered output. Based on these key points, the jumping parameters can be calculated which are then in a last stage saved to a hdf5 file as well as used for the automatic takeoff frame detection.

The whole process is visualized below in Figure 4.2.

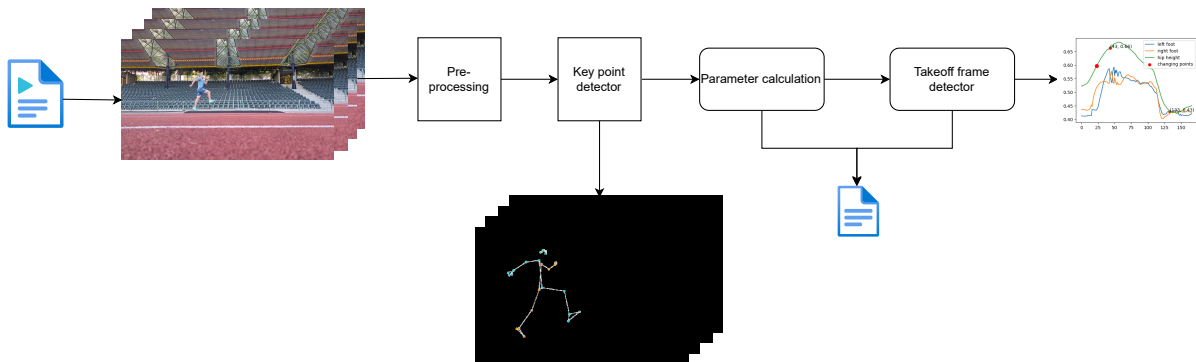


Figure 4.2: Video processing pipeline.
 Stages, that each video frame passes through.

In the following subsections each of the shown processing stages will be explained in detail.

Pre-processing via filter application

The first stage is meant to prepare the incoming video frames to get the best possible result from the following pose detection stage. Thus, this stage will in the following be referred to as *pre processing stage*.

To get an accurate pose detection result it is important to have sharp edges around the athletes' body and an overall low noise level. This can be achieved by applying different filters to each frame.

Three of the most commonly used filters are high-pass (sharpening), low-pass (blurring) and edge preserving low-pass filters, also known as bilateral filters. As the best choice depends on the video input and recording conditions, all of them are implemented and can be mixed with each other.

The low- and high pass filter operations can be expressed as 2D spatial convolutions of an input image \mathbf{I} of size (x_i, y_i) and a (quadratic) filter kernel \mathbf{K} of size (x_k, y_k) .

$$C(i, j) = \sum_{m=-a}^a \sum_{n=-b}^b K(m, n) \cdot I(i - m, j - n) \quad (4.1)$$

where C is the filtered output frame, $a = \lfloor \frac{x_k}{2} \rfloor$ and $b = \lfloor \frac{x_i}{2} \rfloor$. This method is also known as moving window filtering and is supported by opencv using the `filter2D()` method.

The low pass filter especially helps to reduce noise in an input video frame. Because of its' blurring character, the edges around the athletes' body lose their details as well. However, especially in low light conditions, this can be a good first approach to get better results from the key point detector stage. The high pass filter on the other hand is not suitable for videos that contain noisy frames. The noise would be amplified as well as the edges which leads to a worse body key point detection performance. However, in high quality video recordings, the high pass filter helps to enhance the overall sharpness and therefore especially the edges around the athletes' body.

To reduce the overall noise level in a video frame while preserving edges, a third filter, namely the *bilateral filter*, is implemented. It is defined by the following equation:

$$C(I)_p = \frac{1}{W_p} \sum_{q \in S} G_{\sigma_s}(\|p - q\|) G_{\sigma_r}(I_p - I_q) I_q \quad (4.2)$$

where $C(I)_p$ is the output intensity of the filtered pixel p . G_{σ_s} is a spatial gauss filter which decreases the influence of pixel q with increasing distance between p and q . G_{σ_r} is a range gauss filter, meaning it decreases the influence of pixel q with increasing intensity difference between p and q . Their intensities are denoted as I_q and I_p respectively. S represents the set of pixels close to p and is determined by a diameter d around each pixel. The normalization factor W_p is given by:

$$W_p = \sum_{q \in S} G_{\sigma_s}(\|p - q\|) G_{\sigma_r}(I_p - I_q) \quad (4.3)$$

Compared to a simple low pass filter, which is as well implemented as gaussian filter, the bilateral filter takes advantage of not only considering the spatial relation between a pixel and its neighbors but also the relation between their intensity values. This allows a bilateral filter not only to smoothen high frequencies, but to preserve sharp edges at the same time. Opencv offers the built-in method `bilateralFilter()` to apply a bilateral filter to an input video frame. Besides the frame that should be filtered, it also takes σ_s and σ_r as parameters, which define the algorithms' sensitivity to spatial- and intensity changes as well as the diameter d in pixels.

As the filters time complexity depends on the region around each pixel that is taken into account in the gaussian weighting process, it is implemented as first approach to smoothen an input video frame without losing important details in the regions relevant for the body key point detection.

Detecting body key points

Each pre processed video frame is passed to the key point detector stage. This stage is based on the mediapipe pose detection framework (see subsection 3.1.2 and subsection 3.1.3). The models used in this work are the BlazePose models. BlazePose is a convolutional neural network with an architecture similar to MobileNetV2.

It is capable of detecting a total of 33 body key points (shown in Figure 3.1). All of them are tried to be detected in each frame, while only few of them are used in the following parameter calculation process.

The BlazePose network is able to work directly with RGB images as. Thus, the filtered results from the pre-processing stage are as well in the RGB color space. The output generally is a 5-tuple for each detected key point. Besides x and y coordinates, BlazePose also offers a depth estimation and values describing the probability of a key point being present and visible in the current frame. The x and y values are normalized according to the image width and height. Furthermore, BlazePose offers three different models¹ which differ in the amount of parameters, thus in the networks' complexity and the resulting detection accuracy. Their inference times range from 0.02s to 0.25s per input video frame respectively. Hence, the least complex model can also be used for real time pose detection. This project supports all three models, as a quick and less accurate analysis can be sufficient (especially in good lighting and recording conditions), whereas the best detection results, especially in poor quality videos are achieved by using the heavy model.

The detected poses can be visualized as can be seen in following Figure 4.3:

¹light, full and heavy



(a) Sample input frame

(b) Pose detection output

Figure 4.3: Sample pose detection output.

(a) is the input video frame and (b) is the pose detector output. The input frame was pre processed using a high pass filter.

Arm- and knee angle calculation

Based on the previously detected body key points, the parameters shown in Figure 4.1 can be calculated. Especially knee angles during the run up- and takeoff phase can give important insights into an athletes' overall jumping dynamics. On this occasion lower knee angles during the run up (toe off point) as well as during the takeoff (swing leg) were found to lead to better jumping results. Thus, theses parameters are calculated by the software and can be saved and visualized afterwards. In the following, the angle calculation is explained based on the knee angle calculation. Taking the relevant detected key points into consideration, following situation is given:

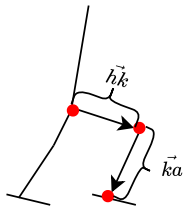


Figure 4.4: Knee angle calculation and related body key points.

Red dots represent the body key points needed to calculate the knee angle. \vec{hk} and \vec{ka} denote the hip-knee vector and the knee-ankle vector respectively.

The vectors \vec{hk} and \vec{ka} can be calculated using the detected key points' coordinates:

$$\vec{hk} = \begin{bmatrix} knee.x - hip.x \\ knee.y - hip.y \end{bmatrix} \text{ and } \vec{ka} = \begin{bmatrix} ankle.x - knee.x \\ ankle.y - knee.y \end{bmatrix} \quad (4.4)$$

Where `.x` and `.y` denote the key points' respective x and y coordinates.

The knee angle θ_{knee} is then represented by the angle between \vec{hk} and \vec{ka} and can be calculated by using the scalar product of \vec{hk} and \vec{ka} and their norms (lengths):

$$\theta_{knee} = \arccos\left(\frac{\vec{hk} \cdot \vec{ka}}{|\vec{hk}| \cdot |\vec{ka}|}\right) \quad (4.5)$$

where \cdot defines the scalar product in this case. The scalar product and the norm are calculated using numpy's `dot()` and `norm()` methods.

The arm angle calculation is performed analogously and is therefore not shown in detail. As the knee- and arm angle calculations have to be done for each video frame, they have to be implemented efficiently not to negatively influence the overall analysis time. Thus, numpy is used to perform the calculations.

Listing 4.1: Angle calculation

```
def calc_angle(first_vec, second_vec):
    [...]
    first_vec_norm = np.linalg.norm(first_vec)
    second_vec_norm = np.linalg.norm(second_vec)
    if first_vec_norm == 0 or second_vec_norm == 0:
        return np.nan
    return 180 - np.rad2deg(
        np.arccos(
            (np.dot(first_vec, second_vec))
            / (first_vec_norm * second_vec_norm)
        )
    )
```

The above shown `calc_angle()` function takes the two vectors as arguments between which the angle should be calculated. These vectors are, in case of the arm- and knee angles, given by the detected body key point positions (see section 4.1.1 and Equation 4.4). By using this implementation the overall angle calculation is sufficient fast (performance analysis are shown in subsection 4.1.3) in comparison to the keypoint detection process in order to allow for a quick on-field analysis.

Takeoff angle calculation

As can be seen in Figure 4.1, in the moment of the takeoff, the Center of mass (CM)'s vertical velocity changes its direction rapidly. This change can be quantised by the angle around which the overall velocity vector rotates. The calculated angle is in the following referred to as *takeoff angle* which is one of the most important pre-jump parameters. As

shown in [10], even small deviations of around 1° of the optimal takeoff angle can lead to shorter measured distances (see Figure 4.1) of up to 5 cm. The optimum takeoff angle differs between athletes and is especially correlated to the takeoff speed [11].

To calculate the takeoff angle, two vectors are needed. The first vector is a horizontal vector origin in the athletes CM. The second vector represents the athletes' CM velocity. It is calculated based on the takeoff frame, which needs to be determined first (see subsection 4.1.2). The second frame which is used to calculate the velocity vector is chosen according to an offset f based on the videos' frame rate². The CM's velocity vector is therefore given by:

$$\vec{v}_t = \frac{1}{f} * (\vec{x}_{t+f} - \vec{x}_t) \quad (4.6)$$

where f is the frame offset and \vec{x}_i are the position vectors. Here, \vec{x}_t represents the CM position at the moment of the takeoff whereas \vec{x}_{t+f} denotes the CM position f frames later. Equation 4.5 can then be applied again yielding following equation for the takeoff angle:

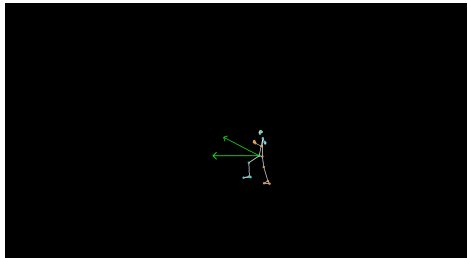
$$\theta_{\text{takeoff}} = \arccos\left(\frac{\vec{v}_t \cdot \vec{h}_t}{|\vec{v}_t| \cdot |\vec{h}_t|}\right) \quad (4.7)$$

where \vec{h}_t denotes any horizontal vector, e.g. $\vec{h}_t = [1, 0]$.

Equation 4.7 is calculated by using the function shown in Listing 4.1 by passing the two vectors shown in following Figure 4.5:



(a) Poses shown as overlay



(b) Extracted vectors and positions

Figure 4.5: Takeoff frame annotated with the **two vectors** that define the takeoff angle marked green.

The horizontal vector in above Figure 4.5 represents \vec{h}_t in Equation 4.7 and the other vector visualizes \vec{v}_t respectively. Moreover, the velocity vector is scaled by a factor of 20 due to visualization reasons.

²Chosen as 1/10 of the frame rate

Saving analysis results

4.1.2 Automatic takeoff frame detection

Generally, a long jump can be divided into three different phases, namely approach, jump and landing. In Figure 4.1 an overview over the phases is given, where the takeoff phase is represented by the first phase changing point.

Each phase demands different requirements from an athlete, however, the takeoff phase is the last phase in which an athlete is able to actively influence the most important jumping conditions. Within this short³ time period the initial kinetic run-up energy is transformed into jumping energy. Especially the velocity vector of an athletes' CM changes its direction in the moment of the takeoff, as illustrated in Figure 4.1. The forces produced during the takeoff strongly influence the resulting jumping distance. Thus, it is important to understand its dynamics.

Due to the short time period a takeoff takes, it can be difficult to detect the takeoff frame in a long jump video in order to be able to analyze the exact pre-jump conditions.

However, especially to allow for an on-field jumping analysis, a quick takeoff frame detection is crucial. Thus, an algorithm that can automatically detect the takeoff frame in a long jump video is implemented in the following.

As the automatic takeoff frame detection is based on the parameters listed in section 4.1, the left and right foot position as well as the position of the CM were analyzed in pre-recorded long jump videos of male long jumpers at different professional levels reaching from hobby- to olympian athlete. Moreover, the videos used differ in their length and quality as well as in the jumping part they show (e.g. video 2 does not show the full run-up). The results of three exemplary video analysis are shown in Figure 4.6. In order to develop an accurate takeoff point detection, the takeoff frame was first manually selected (marked as [blue vertical line](#) for each analysis in Figure 4.6).

The presented data has not been cleaned up in any way. This can especially be seen in the first and last analysis, in which the position and angle data is not accurate due to body key point detection inaccuracies. These inaccuracies however are not of great interest as the key points are detected correctly during the approach after a few frames.

In each analysis the left and right foot positions as well as the according knee angles interchange from step to step. The relative CM height remains on the same level during the approach.

³0.1s 0.2s[12]

Behind the takeoff point, the relative hip- and foot heights increase quickly until the maximal height is reached and the landing phase starts. Moreover, the swing legs' foot height increases faster in comparison to the jumping legs' foot height as the latter one stays on the ground longer to introduce the jump.

In the moment of the takeoff, the knee angle of the jumping leg is above 170 degree, meaning the jumping leg is fully extended. The swing legs' knee angle varies in the shown examples around 100 degree.

The visually most significant change which happens in the moment of the takeoff and is therefore the most meaningful measured parameter that indicates the takeoff is CM's rapid height change. Thus, the automatic takeoff detection is developed based on this parameter.

To approach the detection of the change in the CMs' vertical velocity, a mathematical description of its position during the jump is modelled.

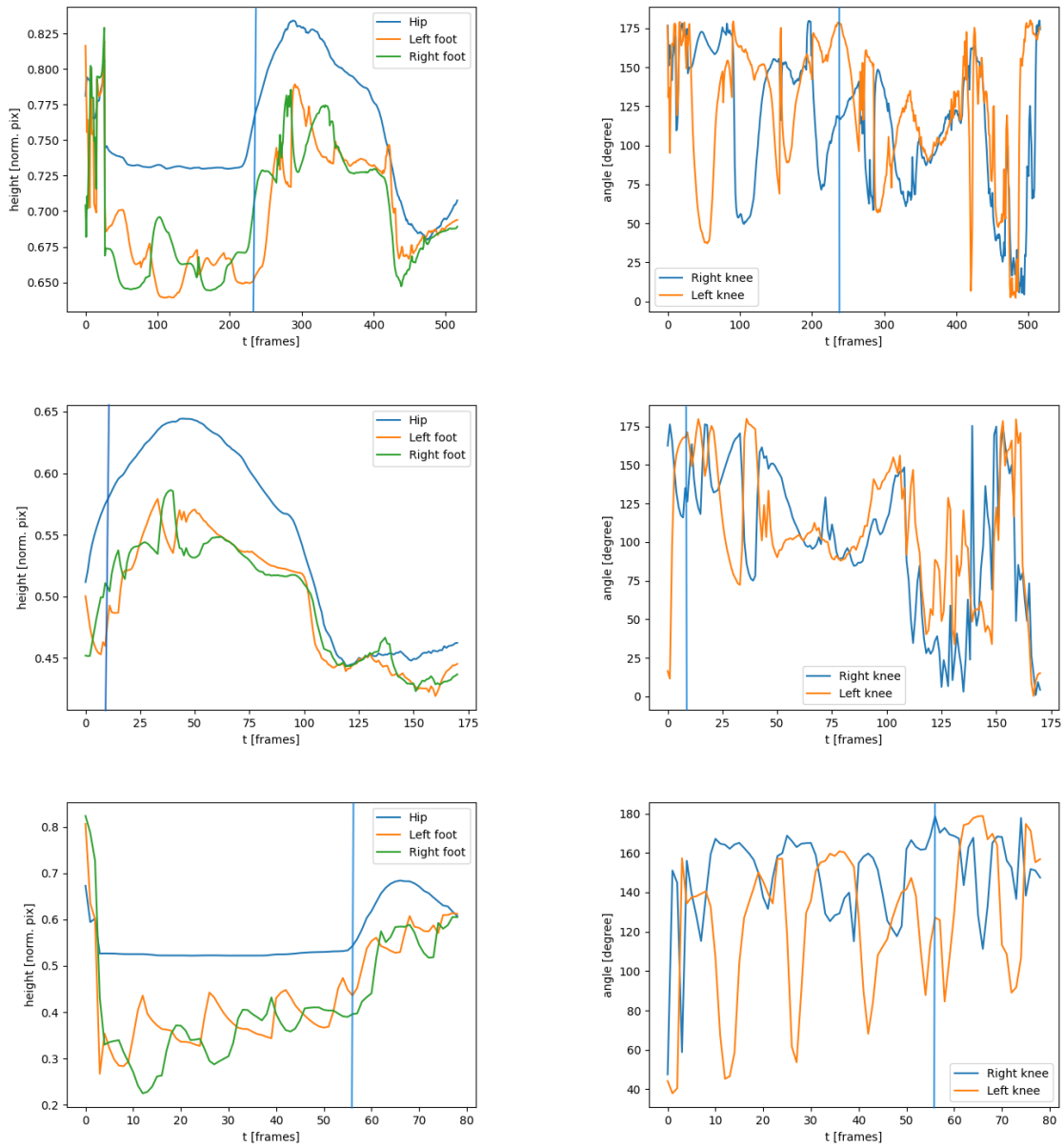


Figure 4.6: Analyzed and calculated jumping parameters over time.

Left column: Analyzed left / right foot height and hip height.

Right column: Calculated knee angles over time.

The [vertical lines](#) represent the visually selected takeoff point.

First row: full run-up, full jump. **Second Row:** short run-up, full jump.

Third row: full run-up, full jump, poor video quality

Regression

As the takeoff point detection is based on linear and quadratic regression, both are briefly introduced in the following. Regression generally describes the approximation of a polynomial function to fit a given dataset. The dataset that is tried to be approximated

in this case is the height of the CM. The dataset can be expressed as (T, H) , where H holds the heights of the CM and T holds the related time points. As the input is a video, T represents a simple vector holding the video's frame numbers. For the following steps it is helpful to express T and H as column vectors:

$$\vec{t} = \begin{bmatrix} 1 \\ 2 \\ \vdots \\ n \end{bmatrix} \quad \text{and} \quad \vec{h} = \begin{bmatrix} h_1 \\ h_2 \\ \vdots \\ h_n \end{bmatrix} \quad (4.8)$$

where n is the total number of video frames and h_i is the i -th recorded height of the CM. Taking the CM in Figure 4.6 into consideration, a whole jump can hardly be fitted with a single polynomial function. However, as shown in Figure 4.1, a long jump consists of multiple phases.

This offers an opportunity to detect the takeoff. As mentioned before, the takeoff frame is defined as the point where the approach phase ends and the jumping phase starts, (PT_0 in Figure 4.1). Thus, if a mathematical expression can be found for each phase respectively, the takeoff frame is found implicitly. The algorithm used for this task is based on the algorithm for a takeoff frame detection developed by Muniz [13].

Other than supposed in his work, the detection algorithm in this work is not based on the foot positions, but on the CM position. There are several reasons for preferring the CM over the foot positions. One of the most important reasons lies in the different jumping techniques, more specifically in the resulting differences during the jumping phase. While the foot path during the jumping phase is rather smooth for athletes using the *hang technique*, it is very different for athletes using the *hitch-kick technique*. Latter one is characterized by quick foot position interchanges, making it more error-prone for inaccuracies in the corresponding body key point detection. Thus, approximating the jumping phase based on the foot positions is more complex and less precise. The CM however follows a similar path independent from the jumping technique, making it more suitable for the given purpose of detecting the takeoff frame.

In the following, the algorithm is explained in detail. All mentioned frame numbers and jumping phases refer to Figure 4.1.

The runup phase includes all frames in the interval $[0, PT_0[$, the jumping phase is covered by the frames in range $[PT_0, PT_1[$ and the landing phase is shown by the frames in the interval $[PT_1, n[$, where PT_0 defines the first Phase Transition point (the takeoff) and PT_1 the point at which the landing phase starts. Each phase by itself can be approximated by a

polynomial function. The approach and the landing can be fitted using a linear expression. Thus, two linear regressions are performed separately to find two expressions of the form

$$y_i = \beta_0 + \beta_1 t_i + \epsilon_i \quad i = \text{start}, \dots, \text{end} \quad (4.9)$$

where β_0 and β_1 are the coefficients that need to be found. *start* and *end* represent the first and last frame index that should be considered in the linear regression. For the approach phase this leads to *start* = 0 and *end* = $TP_0 - 1$, the landing phase is accordingly represented by *start* = TP_1 and *end* = $n - 1$.

Equation 4.9 can also be expressed as matrix equation:

$$\underbrace{\begin{bmatrix} y_0 \\ y_1 \\ \vdots \\ y_r \end{bmatrix}}_{\vec{y}} = \underbrace{\begin{bmatrix} 1 & t_{\text{start}} \\ 1 & t_{\text{start}+1} \\ \vdots & \vdots \\ 1 & t_{\text{end}} \end{bmatrix}}_{\substack{\text{Design matrix} \\ T}} \underbrace{\begin{bmatrix} \beta_0 \\ \beta_1 \end{bmatrix}}_{\vec{\beta}} + \underbrace{\begin{bmatrix} \epsilon_0 \\ \epsilon_1 \end{bmatrix}}_{\vec{\epsilon}} \quad (4.10)$$

where $r = \text{end} - \text{start}$. This can be written in short form as:

$$\vec{y} = T \vec{\beta} + \vec{\epsilon}$$

Now, the vector $\vec{\beta}$ needs to be found that minimizes the sum of errors E_{SSE} between the measured CM heights $h_i \in \vec{h}$ and the fitted polynomial y_i at time step i . To measure the error, the Sum of Squared Errors (SSE) is used:

$$E_{SSE} = \sum_{i=\text{start}}^{\text{end}} \epsilon_i^2 = \sum_{i=\text{start}}^{\text{end}} (h_i - y_i)^2 \quad (4.11)$$

Using the simple linear expression from Equation 4.9, following error function is found:

$$E_{SSE} = \sum_{i=\text{start}}^{\text{end}} (h_i - \beta_0 - \beta_1 i)^2 \quad (4.12)$$

By using the matrix notation introduced in Equation 4.10, the equation above can be written in matrix notation as well:

$$E_{SSE} = (T \vec{\beta} - \vec{h})^T (T \vec{\beta} - \vec{h}) \quad (4.13)$$

As $\vec{\beta}$ should minimize E_{SSE} , the minimum of E_{SSE} is needed, which can be found by solving following equation:

$$\nabla_{\vec{\beta}} E_{SSE} = \nabla_{\vec{\beta}} (T\vec{\beta} - \vec{h})^T (T\vec{\beta} - \vec{h}) = 0 \quad (4.14)$$

where $\nabla_{\vec{\beta}}$ denotes the gradient with respect to $\vec{\beta}$.

The coefficients can then be found by solving Equation 4.14 for $\vec{\beta}$, which yields the following normal equation:

$$\vec{\beta} = (T^T T)^{-1} (T^T \vec{h}) \quad (4.15)$$

that especially requires $(T^T T)$ to be invertible. A proof of Equation 4.15 can be found in [14].

As mentioned, this process is performed twice to find a linear approximation for the approach and the landing phase of an athletes' CM respectively.

The jumping phase cannot be approximated with a linear polynomial. However, as can be seen in Figure 4.6 after the marked takeoff point, the curve of the CM height can be approximated using a parabola. Thus, quadratic regression is used to find a curve that describes the height of the CM during the jumping phase. The second order polynomial that needs to be found is of the form:

$$y_i = \beta_0 + \beta_1 t_i + \beta_2 t_i^2 + \epsilon_i \quad i = PT_0, \dots, PT_1 - 1 \quad (4.16)$$

PT_0 and PT_1 are the phase transition points shown in Figure 4.1. The following steps are equal to the linear regression shown above. Thus, only the differences are shown in detail. The T matrix in Equation 4.10 contains all frame numbers as column vector. Because a linear relation was tried to be found to approximate the approach and landing phase before, the T matrix as well only contained linear values. Now however, a quadratic relation needs to be found. Thus, the T matrix needs to be extended by one more column holding the quadratic frame numbers yielding following matrix equation:

$$\underbrace{\begin{bmatrix} y_0 \\ y_1 \\ \vdots \\ y_r \end{bmatrix}}_{\vec{y}} = \underbrace{\begin{bmatrix} 1 & t_{PT_0} & t_{PT_0}^2 \\ 1 & t_{PT_0+1} & t_{PT_0+1}^2 \\ \vdots & \vdots & \vdots \\ 1 & t_{PT_1-1} & t_{PT_1-1}^2 \end{bmatrix}}_T \underbrace{\begin{bmatrix} \beta_0 \\ \beta_1 \\ \beta_2 \end{bmatrix}}_{\vec{\beta}} + \underbrace{\begin{bmatrix} \epsilon_0 \\ \epsilon_1 \\ \vdots \\ \epsilon_2 \end{bmatrix}}_{\vec{\epsilon}} \quad (4.17)$$

where $r = PT_1 - 1 - PT_0$. The error function which needs to be minimized can be set equivalent to the linear case (Equation 4.13). Comparing Equation 4.10 and Equation 4.17

the only things that change are the number of coefficients (and thus the number of error terms) as well as the design matrix T , which holds one more column. The steps to determine the coefficients $\vec{\beta}$ are equal to the linear case in equations 4.13 to 4.15. $\vec{\beta}$ is then given by the same normal equation 4.15 as in the linear case:

$$\vec{\beta} = (T^T T)^{-1} (T^T \vec{h})$$

where $\vec{\beta}$ contains three coefficients β_0 , β_1 and β_2 to approximate the jumping phase.

By using this linear- and quadratic regression approach, the whole jump can be modelled mathematically. However, in order to find the best fitting model, the phase changing points (PT_0 and PT_1 in Figure 4.1) need to be determined. This can be done by minimizing the overall error E_{total} , which is defined as the sum of regression errors resulting from the three independent regressions performed (one per jumping phase):

$$E_{total} = E_{approach} + E_{jump} + E_{landing} \quad (4.18)$$

E_{total} can be minimized by using a brute-force approach. For each possible combination of phase transition points, two linear regressions (representing approach and landing) and one quadratic regression (representing the jumping phase) are performed and their individual errors given by Equation 4.13 are summed up. The combination of phase transition points that leads to the minimal E_{total} is then considered as the optimal model to fit the overall jump. As the found phase transition points directly represent their corresponding frame numbers, the takeoff frame is directly given by the first phase transition point.

The described process is outlined in following Algorithm 1.

Algorithm 1 takeoff_frame(cm_height: array, knee_angles: array)

```

1:  $n \leftarrow$  length of  $cm\_height$ 
2:  $total\_error \leftarrow$  initial error
3:  $transition\_points \leftarrow (0, 0)$ 
4: for  $i \leftarrow 0$  to  $n - 1$  do
5:   for  $j \leftarrow i + 1$  to  $n$  do
6:      $\beta_{approach}, error\_approach \leftarrow lin\_reg(hip\_height[:i])$ 
7:      $\beta_{jump}, error\_jump \leftarrow quad\_reg(hip\_height[i:j])$ 
8:      $\beta_{landing}, error\_landing \leftarrow lin\_reg(hip\_height[j:])$ 
9:      $fitting\_error \leftarrow error\_approach + error\_jump + error\_landing$ 
10:    if  $fitting\_error < total\_error$  and  $\beta_{jump}[0] < 0$  and  $knee\_angles[i] > 170$  then
11:       $total\_error \leftarrow fitting\_error$ 
12:       $transition\_points \leftarrow (i, j)$ 
13:    end if
14:  end for
15: end for
16: return  $transition\_points$ 

```

The expression $\beta_{jump}[0] < 0$ guarantees, that the found parabola for approximating the jumping phase is opened downwards. Moreover, $knee_angles[i] > 170$ makes sure, that only frames in which the knee angle is above 170 degrees can be considered as takeoff point.

The shown algorithms' runtime scales according to $\mathcal{O}(n^2)$ where n is the number of video frames⁴. Thus, it is not suitable for long video sequences. However, as a complete long jump takes only a few seconds, the algorithm can be used for an on-field jump analysis. Algorithm 1 was then applied to all three datasets shown in Figure 4.6. The results are shown in Figure 4.7.

For better understanding, the height of the CM was extracted from the datasets as it is the only parameter relevant for the takeoff detection. The data is not cleaned up in any way, thus, outliers are still visible. However, as can be seen, the automatically detected takeoff frames are similar to the manually annotated frame numbers.

⁴in which body key points were found

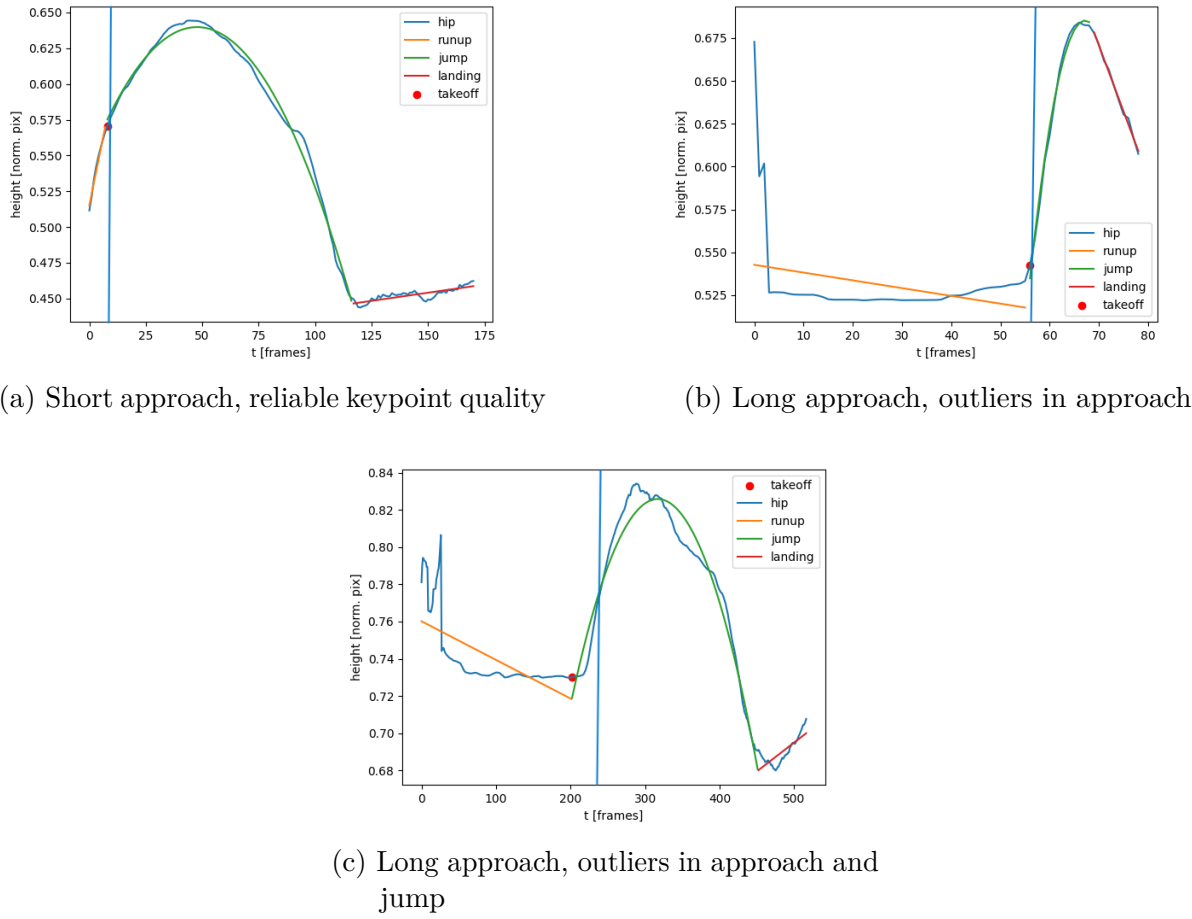


Figure 4.7: All three jumping phases approximated using linear regression (runup and landing) and quadratic regression (jumping phase).

The automatically detected takeoff frame is marked with a **red dot**.

The **vertical blue lines** represent the manually marked takeoff frames.

4.1.3 Runtime considerations

4.1.4 Visualization in a GUI

4.2 Hardware setup

In order to capture high-quality video recordings that cover a complete long jump, from the first step all the way to the landing, a drone is used to fly next to the athlete throughout the whole process. Thus, a drone in form of a quadcopter is built from scratch. Its control will be integrated seamlessly in the projects' GUI.

This section introduces the hardware components that are used for building this drone as well as its flight control unit.

A short outline of the hardware is given in subsection 4.2.1, while subsection 4.2.2 focuses on the overall assembly of the selected hardware.

4.2.1 Hardware selection

Currently, commercial drone hardware on the market is mainly separable into the two large areas of fully remote controlled FPV hardware and hardware for (autonomous) drones that can usually carry more load, e.g. heavy cameras. Even though the quadcopter in this project needs to be remotely controllable from a ground station pc, it is still more likely to be located in the latter one.

Generally the hardware was chosen based on the following criteria:

- price
- compatibility
- size

Flight Hardware

The main hardware that a quadcopter needs to fly will, in the following, be referred to as *flight hardware*. This includes frame, motors, rotors, Electronic Speed Controls (ESCs) and a Power Delivery board (PDB).

The main platform on which all drone hardware is mounted, is referred to as a quadcopter's frame. As this project's drone does not need to carry any heavy load, such as high precision camera systems or other sensors, a rather compact frame would theoretically be sufficient. However, compact frames tend to be less stable compared to larger frame sizes which could lead to a lower video recording quality and thus require more complex post-processing software. Moreover, the assembly process on larger frames is more convenient and replacing parts is easier. Additionally, compact frames are most commonly used in areas that demand quick reaction times for high speed flight maneuvers, e.g. in drone racing. This however is not needed in this project's context.

Taken the mentioned considerations into account the mid-sizes *Holybro S500 V2* frame kit is chosen. Besides the frame, the kit also includes a landing gear and rotors. Moreover, the main platform includes a PDB to split the battery's power equally to all four motors. An overview of all included parts is given in Figure 4.8.



Figure 4.8: Holybro S500 V2 frame kit

Besides the frame, motors and compatible ESCs are crucial flight hardware components. Each motor requires an own ESC that translates signals from a flight control unit to a voltage and thereby control the motors' rotation speed. To guarantee compatibility, both components were chosen from Holybro as well and can be seen in Figure 4.9.



(a) 920KV Motor

(b) Electronic Speed Control

Figure 4.9: Motor (a) and ESC (b)

The drones' motors performance capabilities are defined by the number of Revolutions Per Minute (RPM) they can perform per 1V input. As can be seen in Figure 4.9a, this link between rotation speed and input voltage is expressed in the arbitrary unit *KV*. The chosen motors are capable of rotating with a speed of 920 RPM per 1V input voltage. Put into context, this is a common rotation speed in commercial and hobby drone applications. Racing drones however, operate at motor speeds of up to 3500 KV.

Control Hardware

In order to perform flight maneuvers with a quadcopter, each motor must be controllable individually. The calculation of the correct rotation speeds is generally performed by a *flight control unit*. Usually, it receives directional instructions from a remote control as input, combines them with many parameters (e.g. GPS position, height over ground, speed, etc.) and generates a (PWM) output signal for each motor.

Within this project the flight controller needs to deal with two different inputs. First, the ground station which can be seen as a remote control in this case. Additionally, the drone should be able to fly autonomously next to an athlete during their long jump training. Here, the second input gets important. The autonomous fly option requires the quadcopter to perform a person detection and therefore image processing on-board. As the flight controller itself is not able to perform such calculations, an additional *companion computer* is required. This companion computer will then send directional instructions just like the ones from the ground station to the flight controller and thereby control the drone.

The combination of flight controller and on-board companion computer will in the following be called *control hardware*.

There are many types of different flight controllers available commercially. However, most of them are not meant to be used in combination with a companion computer.

Two of the most commonly used flight controllers in autonomous drone projects are the *PixHawk* and the *Navio2*. They are often chosen because they both work together seamlessly with a companion computer. The former is a totally independent system which can also operate without any supporting computer. The latter is implemented as Hardware Attached on Top (HAT) specifically designed for a Raspberry Pi. Thus, it does not include an own CPU but uses the Raspberry Pi's resources to perform flight relevant calculations. A detailed comparison between both flight controllers is given in Table 4.1.

As can be seen, both flight controllers offer different interfaces to connect additional hardware. Moreover, both systems include sensors, mostly to gather information about drone's current position and inertia. Here, the Navio2 even offers more sensors, as it already includes a Global Positioning System (GPS) sensor, while the PixHawk relies on an external one.

For this project, the PixHawk was chosen over the Navio2 mainly for three reasons. First, it is on the market for a long time already and thus have a large community support. Secondly, as it is an independent system, a failure of the companion computer will not lead to a crash. Lastly, it allows for a wide range of companion computers, while the Navio2 can only interoperate with a Raspberry Pi.

| Flight Controller Comparison | | |
|------------------------------|--|---|
| Criteria | PixHawk | Navio2 |
| Processor | ARM Cortex M4 with FPU / 32-bit co-processor | Depends on Raspberry Pi version |
| Sensors | ST Micro 16-bti gyroscope, ST Micro 14-bit accelerometer, MEAS barometer | MPU9250 9DOF IMU, LSM9DS1 9DOF IMU, MS5611 Barometer, U-blox M8N Glonass/GPS/Beidou |
| Interfaces | UART, Spektrum DSM, PPM / S.BUS input, I2C, SPI, CAN, USB, 3.3V and 6.6V ADC input, 8 PWM outputs, 6 Auxiliary outputs | UART, I2C, ADC, PPM / S.BUS input, 14 PWM outputs |
| Dimensions (W x H x L) in mm | 50 × 15.5 × 81.5 | 55 × 65 |
| Other | Failsafe options (e.g. extra power supply, GPS, etc.) | None |
| Price (Eur.) | TBD | TBD |

Table 4.1: Comparison between PixHawk and Navio2 flight controller.

Furthermore, the mentioned considerations lead to easy rapid prototyping approaches, as the drone can be manually flown without a companion computer in a first implementation.

4.2.2 Hardware assembly

In the following, a high-level overview of the quadcopters' hardware setup is given. The general wiring is shown and explained before a short introduction of some important communication protocols is given.

General wiring

In the following Figure 4.10 the general wiring layout is shown. The whole system is powered from one power source only.

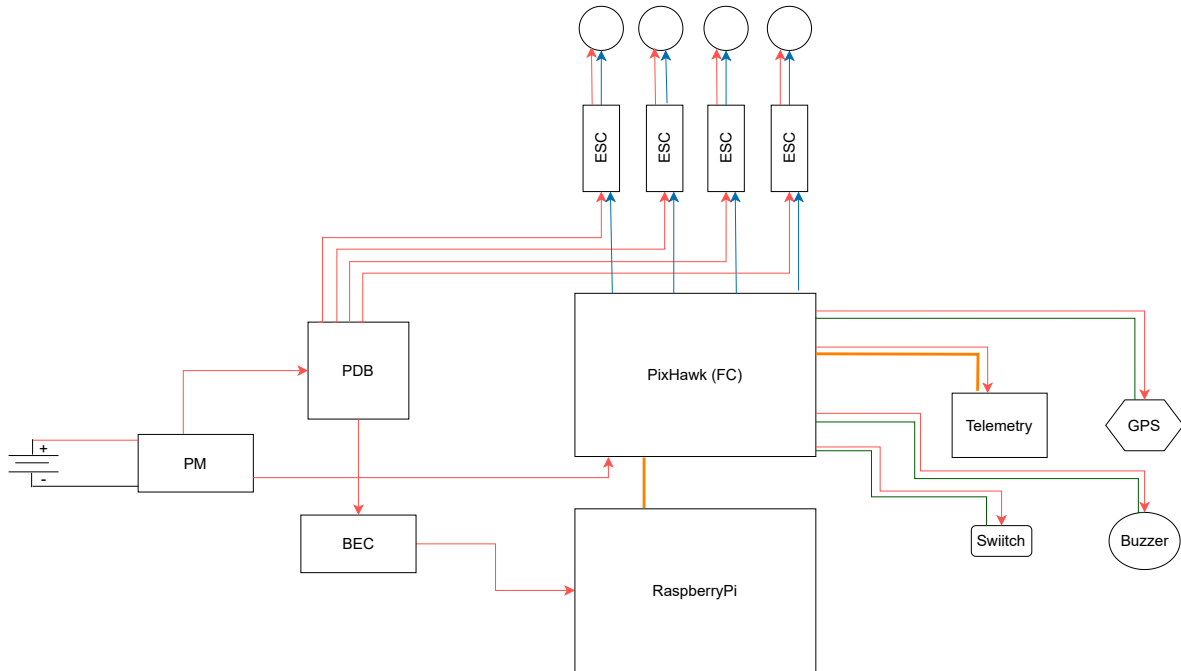


Figure 4.10: General wiring of the hardware setup.

Power connections are labeled red, Blue connections are used for Pulse Width Modulation (PWM) signals, Green connections are serial connections, orange connections are more specifically serial UART connections.

This results in some challenges in providing the correct voltage for each connected device. In the current setup this task is taken over by three devices. The Power Module (PM) is directly connected to the battery. It transfers the battery's voltage to the PDB and a lower 5V voltage to the PixHawk flight controller. The PDB itself is a parallel circuit, thus providing the same voltage (battery voltage) to each output. The third device is a Battery Elimination Circuit (BEC) which is directly connected to the PDB and delivers a constant 5V output. This can be used to power a companion computer such as a RaspberryPi. All other required peripherals are powered by the PixHawk flight controller itself. The main peripherals used in this project are a telemetry module which is used for communication with a ground station and a GPS module used for improving the drone's capabilities to follow a defined trajectory, which is specifically useful for auto-return and landing features. Two more peripherals, a buzzer to output audio warning signals and a manual kill switch which can immediately stop all four motors, are installed mainly for safety reasons. The hardware components that actually control the motor rotation speeds, the ESCs, are connected to the PDB for power supply as well as to the flight controller that calculates the correct rotation speeds based on the wanted flight maneuvers and outputs a PWM signal for each motor.

The presented overall wiring is rather complex but allows relying on one power source only

instead of using multiple power sources for flight hardware and control hardware including peripherals respectively.

Communication between components

The drone setup needs hardware components to communicate with each other in order to transfer control signals from either the companion computer or from the ground station to the flight controller. Even if both options origin from different sources, they use the same device-to-device communication protocol. The protocol used for this purpose is the *UART* protocol, which is acronym for universal asynchronous receiver / transmitter protocol. It is based on a serial, full duplex connection using six connections. The connection layout is shown in Figure 4.11,

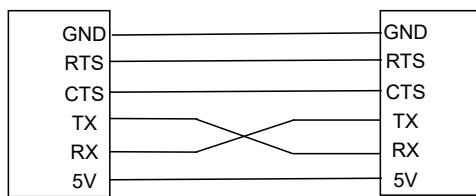


Figure 4.11: UART wiring

where RTS / CTS denote Ready to send and Clear to send. RX / TX represent the actual data receiving and sending connections respectively.

UART transfers data using data frames with minimal overhead. A typical UART frame consists of just a start bit, data bits, a parity bit and a stop bit. Figure 4.12 visualizes such a data frame.

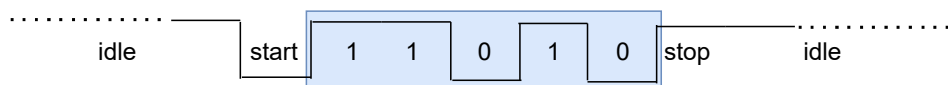


Figure 4.12: Example of an UART data frame. The blue marked area is the actual data part that is transmitted.

The shown UART data frame includes 5 data bits, however, the amount can vary between 5 and 9. Moreover, the included even parity bit is optional. The idle state is set to a voltage that represents HIGH level on purpose, so that any connection failure is easily detectable. UART can work with any voltages to denote HIGH and LOW levels. In the quadcopter setup HIGH is represented by 5V and LOW by GND.

Bibliography

- [1] A. Seyfarth et al. “Dynamics of the long jump”. In: *Journal of Biomechanics* 32.12 (1999), pp. 1259–1267. ISSN: 0021-9290. DOI: [https://doi.org/10.1016/S0021-9290\(99\)00137-2](https://doi.org/10.1016/S0021-9290(99)00137-2). URL: <https://www.sciencedirect.com/science/article/pii/S0021929099001372>.
- [2] Murray Evans et al. “Automatic high fidelity foot contact location and timing for elite sprinting”. In: *Machine Vision and Applications* 32.5 (2021). DOI: 10.1007/s00138-021-01236-z.
- [3] Chang Soon Tony Hii et al. “Marker Free Gait Analysis using Pose Estimation Model”. In: *2022 IEEE 20th Student Conference on Research and Development (SCOReD)*. 2022, pp. 109–113. DOI: 10.1109/SCOReD57082.2022.9974096.
- [4] Valentin Bazarevsky et al. “BlazePose: On-device Real-time Body Pose tracking”. In: *CoRR* abs/2006.10204 (2020). arXiv: 2006.10204. URL: <https://arxiv.org/abs/2006.10204>.
- [5] Amit Gupta et al. “Knee Flexion/Extension Angle Measurement for Gait Analysis Using Machine Learning Solution “MediaPipe Pose” and Its Comparison with Kinovea®”. In: *IOP Conference Series: Materials Science and Engineering* 1279.1 (March 2023). Publisher: IOP Publishing, p. 012004. DOI: 10.1088/1757-899X/1279/1/012004. URL: <https://dx.doi.org/10.1088/1757-899X/1279/1/012004>.
- [6] Google Developers. *Pose landmark detection guide*. 2023. URL: https://developers.google.com/mediapipe/solutions/vision/pose_landmarker (visited on November 5, 2023).
- [7] Zhe Cao et al. “Realtime Multi-Person 2D Pose Estimation using Part Affinity Fields”. In: *CoRR* abs/1611.08050 (2016). arXiv: 1611.08050. URL: <http://arxiv.org/abs/1611.08050>.
- [8] Muhammed Kocabas et al. “MultiPoseNet: Fast Multi-Person Pose Estimation using Pose Residual Network”. In: *Proceedings of the European Conference on Computer Vision (ECCV)*. September 2018.

-
- [9] Daniil Osokin. “Real-time 2D Multi-Person Pose Estimation on CPU: Lightweight OpenPose”. In: *CoRR* abs/1811.12004 (2018). arXiv: 1811 . 12004. URL: <http://arxiv.org/abs/1811.12004>.
 - [10] A. Seyfarth et al. “OPtimum Take-Off Techniques and Muscle Design for Long Jump”. In: *Journal of Experimental Biology* 203.4 (February 15, 2000), pp. 741–750. ISSN: 0022-0949. DOI: 10.1242/jeb.203.4.741. URL: <https://doi.org/10.1242/jeb.203.4.741> (visited on March 3, 2024).
 - [11] Kazuhiro Tsuboi. “A mathematical solution of the optimum takeoff angle in long jump”. In: *Procedia Engineering*. The Engineering of Sport 8 - Engineering Emotion 2.2 (June 1, 2010), pp. 3205–3210. ISSN: 1877-7058. DOI: 10 . 1016 / j . proeng . 2010 . 04 . 133. URL: <https://www.sciencedirect.com/science/article/pii/S1877705810003875> (visited on February 11, 2024).
 - [12] P. Luhtanen and P. V. Komi. “Mechanical power and segmental contribution to force impulses in long jump take-off”. In: *European Journal of Applied Physiology* 41 (1979), pp. 267–274. DOI: 10.1007/BF00429743.
 - [13] Pablo E. (Muñiz Aponte) Muñiz. “Detection of launch frame in long jump videos using computer vision and discreet computation”. Accepted: 2019-12-13T19:02:08Z. Thesis. Massachusetts Institute of Technology, 2019. URL: <https://dspace.mit.edu/handle/1721.1/123277> (visited on February 11, 2024).
 - [14] M. Arioli and S. Gratton. “Linear regression models, least-squares problems, normal equations, and stopping criteria for the conjugate gradient method”. In: *Computer Physics Communications* 183.11 (2012), pp. 2322–2336. ISSN: 0010-4655. DOI: <https://doi.org/10.1016/j.cpc.2012.05.023>.